Effect of Calcium on the Formation and Protectiveness of an Iron Carbonate Layer in CO_2 Corrosion

Saba Navabzadeh Esmaeely, Yoon-Seok Choi, David Young, and Srdjan Nešić, FNACE, *Institute for Corrosion and Multiphase Technology, Ohio University, Athens, Ohio*

Among the known options in carbon capture and storage, the injection and storage of carbon dioxide (CO_2) in deep saline aquifers has the potential to cause casing corrosion due to the direct contact between injected CO_2 and the saline aquifer, which contains highly concentrated aqueous salts such as sodium chloride (NaCl) and calcium chloride ($CaCl_2$). Thus, in the present study, the effect of Ca^{2+} on the CO_2 corrosion behavior of mild steel was investigated in simulated saline aquifer environments. The results show that with low concentrations of Ca^{2+}, the corrosion rate decreased with time due to the formation of protective iron carbonate ($FeCO_3$) and/or $Fe_xCa_yCO_3$ ($x + y = 1$). The presence of high concentrations of Ca^{2+} lead to an increasing corrosion rate with time.

Since carbon dioxide (CO_2) emission is directly proportional to fossil fuel consumption, the capturing and subsequent geologic storage of CO_2 is a candidate technology for controlling its emission.[1] The carbon capture and storage (CCS) process contains three stages: CO_2 capture, transportation to the geologic storage site (usually by pipeline), followed by injection into geologic reservoirs.[2]

Corrosion rates of casing steel are highly dependent on the formation of iron carbonate ($FeCO_3$) in CO_2/saline aquifer environments. Brine species such as Ca^{2+}, which can form carbonate layers/scales, are very important in corrosion studies as they can compete with Fe^{2+} in the formation of carbonates. Therefore, there is a possibility of changing the $FeCO_3$ morphology, composition, and protectiveness in such environments, which can in turn affect general and localized corrosion of casing steel.

Little has been reported in the literature on the effect of Ca^{2+} on corrosion. Xian, et al. claimed that corrosion rate decreased in the short term in the presence of Ca^{2+} and Mg^{2+}, but there was no special difference in long-term exposure.[3-4] Ding, et al. reported the corrosion rate increased with an increase in the Ca^{2+} concentration.[5] Jiang, et al. reported pitting associated with calcium chloride ($CaCl_2$).[6] They claimed that Cl^- caused pitting, but the presence of Ca^{2+} postponed the initiation of the pitting. Ren, et al.,[7] as well as Zhu, et al.,[8] reported pitting with reference to the presence of Cl^- in $CaCl_2$-containing electrolytes. Gao, et al.[9] reported pitting in conjunction with the formation of $Fe_xCa_yCO_3$ and $Fe_x(Mg, Ca)_yCO_3$ ($x + y = 1$) on the steel surface. A broader review of the literature indicates that Cl^- ions are often associated with pitting. The role of overall water chemistry, and Ca^{2+} ions in particular, is generally not clear.

The objective of the present study is to evaluate the effect of Ca^{2+} on the CO_2 corrosion behavior of mild steel in simulated saline aquifer environments related to the injection and storage of CO_2 by conducting well-controlled and thoroughly qualified experiments.

Experimental Setup and Procedure

Experiments were conducted in a 2-L glass cell using a three-electrode setup. In each experiment, three flat specimens made from mild steel (UNS G10180) with an exposed area of 540 mm^2 were used for electrochemical measurement and for surface analysis. Prior to insertion, the specimens were wet-polished with silicon carbide (SiC) paper down to 600 grit, rinsed with isopropyl alcohol in an ultrasonic bath, and dried.

Tables 1 and 2 show the test matrix and test conditions, respectively. The glass cell was filled with 2 L of 1 wt% sodium chloride (NaCl) electrolyte (prepared with deionized water). The solution was stirred with a magnetic stirrer and the temperature was set to 80 °C. CO_2 gas was continuously purged through the solution. The solution pH was adjusted to 6.6 by adding a deoxygenated 1.0 M sodium hydroxide (NaOH) solution. After the pH stabilized, the magnetic stir bar was stopped and samples were inserted into the glass cell.

The corrosion behavior was monitored by electrochemical methods: open circuit potential (OCP) and linear polarization resistance (LPR) measurements. Samples from all experiments were characterized by x-ray diffraction (XRD), scanning electron microscopy (SEM), energy dispersive x-ray spectroscopy (EDS), and infinite focus microscopy (IFM) to investigate the effect of Ca^{2+} on the morphology and composition of the corrosion product layer. The Ca^{2+} concentration was measured using inductively coupled plasma (ICP) spectroscopy. Analyses for the Fe^{2+} concentration were performed with an ultraviolet-visible (UV-Vis) spectrophotometer.

At the end of each experiment and after completion of the corrosion product surface analysis, one sample from each experiment was treated with Clarke solution to remove the corrosion product layer and the underlying metal surface, was scanned in accordance with ASTM G1.[10]

Results

Figure 1 shows the variations of OCP and corrosion rate with time for each experiment condition. As shown in Figure 1(a), the corrosion rate decreased with time for the low initial Ca^{2+} concentration conditions. This indicates that a protective $FeCO_3$ layer was formed on the steel surface.

When a $FeCO_3$ layer forms on the mild steel surface, it can slow down corrosion by presenting a diffusion barrier for the species involved in the process, and by blocking (covering) a portion of the steel surface and preventing the underlying steel from undergoing further oxidative dissolution.[11-12]

For the low initial Ca^{2+} concentration conditions (0, 10, and 100 ppm), the formation of a protective $FeCO_3$ layer apparently occurred without significant interference

TABLE 1. TEST MATRIX

Parameters	Conditions
Total pressure	0.1 MPa
pCO_2	0.05 MPa
Temperature	80 °C
Solution	1 wt% NaCl
pH	6.6
Flow condition	Stagnant
Steel	UNS G10180

TABLE 2. TEST CONDITIONS

Test Condition No.	Initial Concentrations of Fe^{2+} and Ca^{2+}
1	10 ppm Fe^{2+}
2	10 ppm Fe^{2+} + 10 ppm Ca^{2+}
3	10 ppm Fe^{2+} + 100 ppm Ca^{2+}
4	10 ppm Fe^{2+} + 1,000 ppm Ca^{2+}
5	10 ppm Fe^{2+} + 10,000 ppm Ca^{2+}

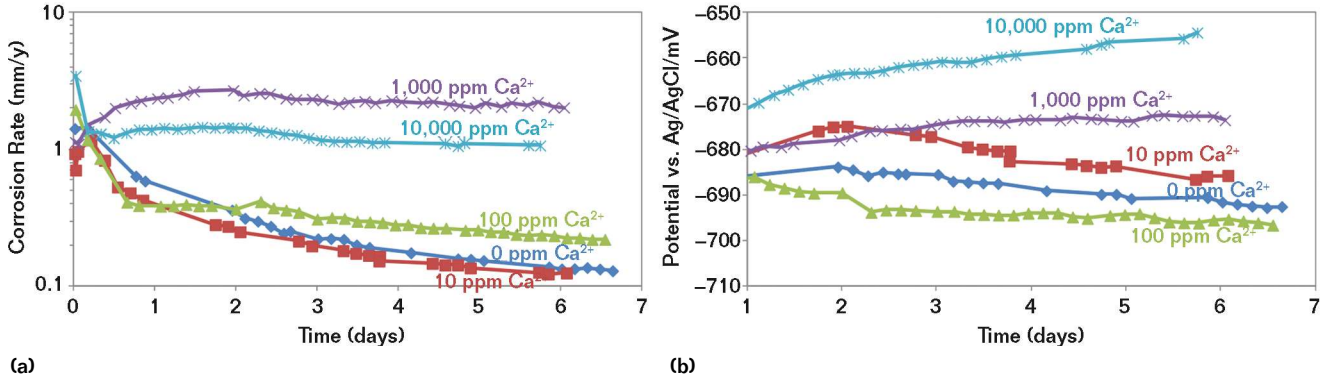

FIGURE 1 Variations of (a) corrosion rate and (b) OCP for mild steel exposed to a simulated brine with different initial concentrations of Ca^{2+} at 80 °C and pCO_2 of 0.05 MPa with 10 ppm Fe^{2+}.

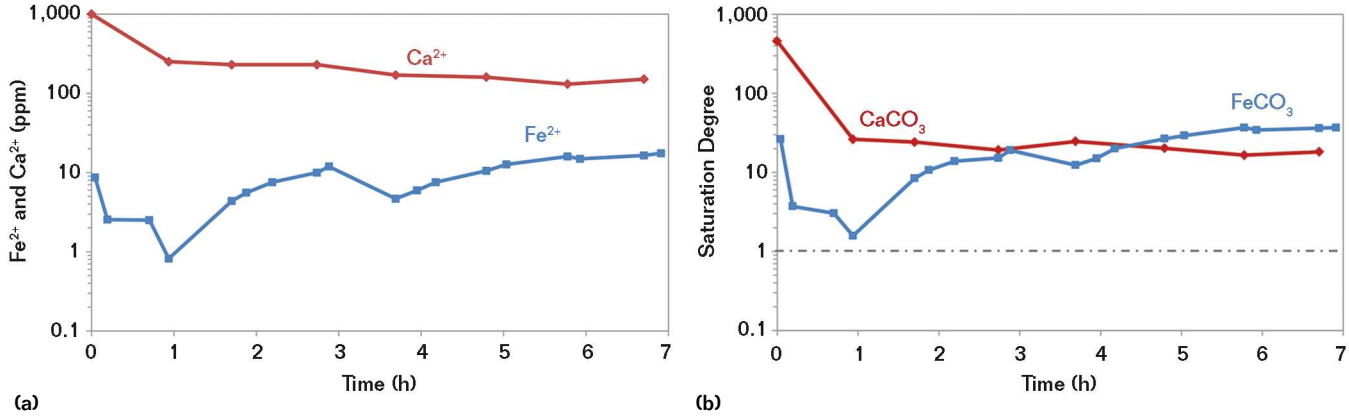

FIGURE 2 (a) Fe^{2+} and Ca^{2+} concentrations and (b) $CaCO_3$ and $FeCO_3$ saturation degree for the initial 1,000 ppm Ca^{2+} system vs. time at 80 °C and pCO_2 of 0.05 MPa with 10 ppm Fe^{2+}.

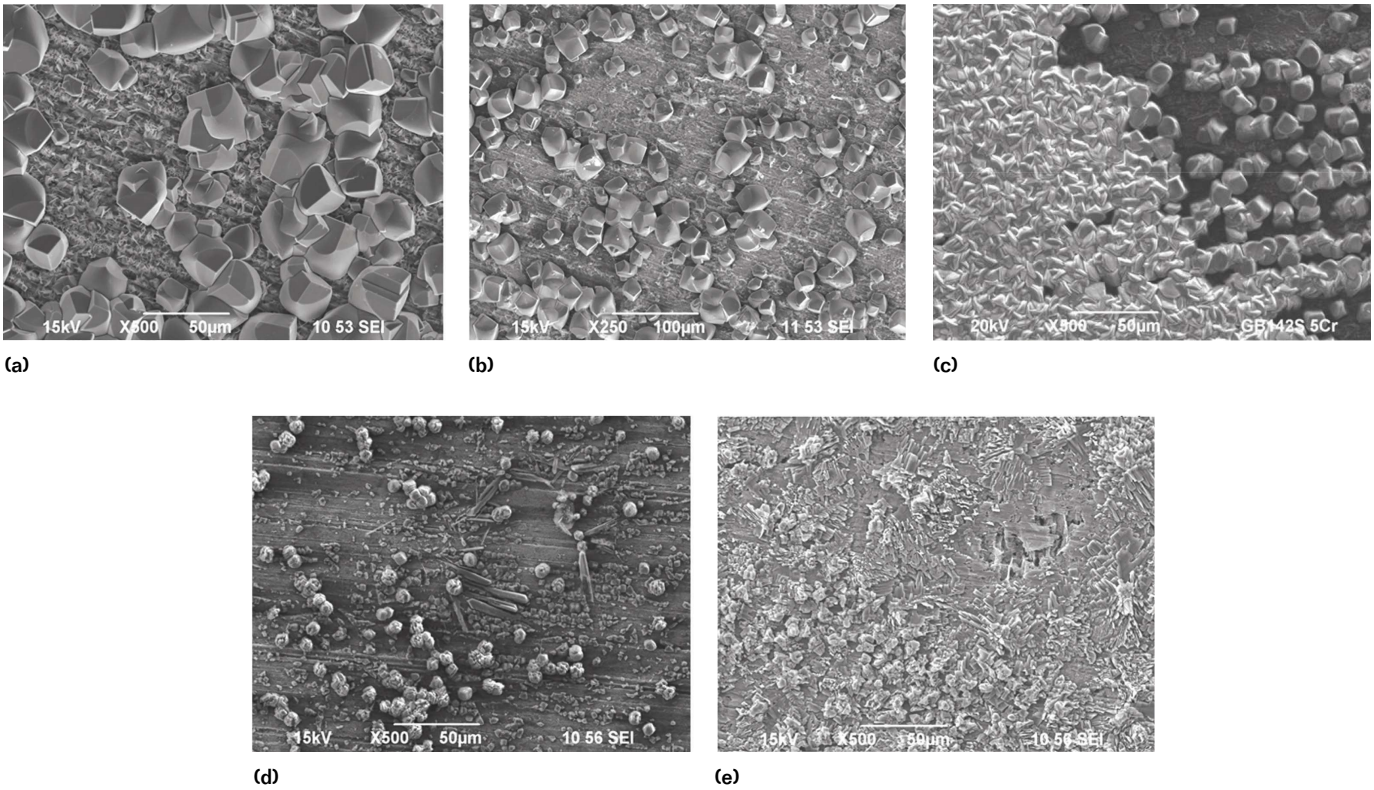

FIGURE 3 SEM images of recovered samples (UNS G10180) from experiments conducted at 80 °C and pCO_2 of 0.05 MPa with 10 ppm Fe^{2+} for (a) 0 ppm Ca^{2+}, (b) 10 ppm Ca^{2+}, (c) 100 ppm Ca^{2+}, (d) 1,000 ppm Ca^{2+}, and (e) 10,000 ppm Ca^{2+}.

by Ca^{2+} ions. However, the corrosion behavior of mild steel with higher initial Ca^{2+} concentrations of 1,000 and 10,000 ppm was different. The corrosion rate did not decrease with time, which is likely due to the lack of formation of a protective $FeCO_3$ layer on the steel surface. At this stage, it can be hypothesized that this was caused by a lower pH seen in experiments with higher initial Ca^{2+} concentrations. Precipitation of calcium carbonate ($CaCO_3$) in aqueous CO_2 solutions will lead to acidification as the equilibrium pH is approached.

The experiments with lower Ca^{2+} concentrations remained highly supersaturated with respect to $FeCO_3$ during the whole experiment, leading to steady precipitation of protective $FeCO_3$. The experiment with initial Ca^{2+} concentration of 1,000 ppm also was supersaturated with respect to $FeCO_3$. At the initial Ca^{2+} concentration of 10,000 ppm, the rapid precipitation of $CaCO_3$ made the solution undersaturated with respect to $FeCO_3$, making

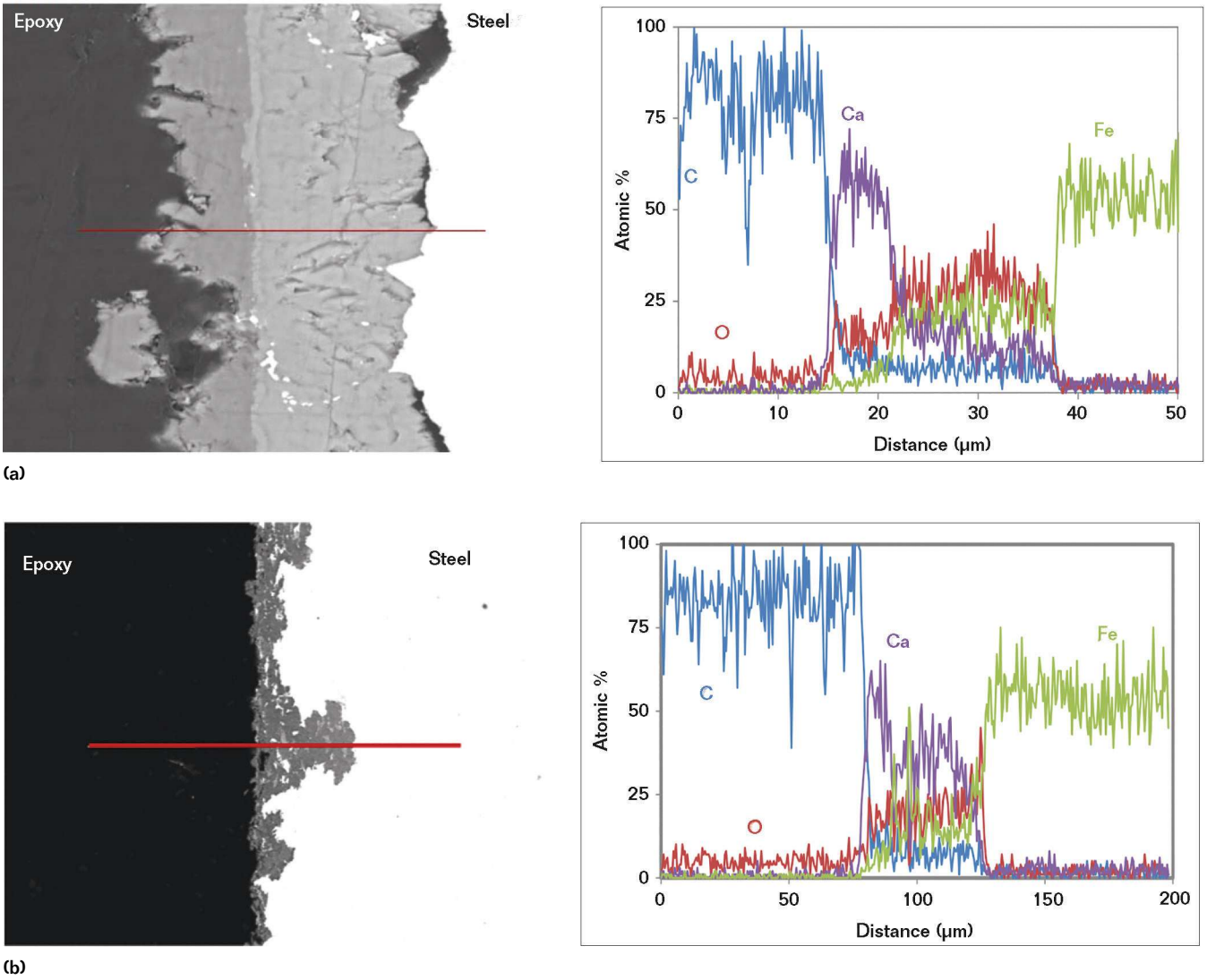

FIGURE 4 Cross section image and EDS spectra of samples (UNS G10180) recovered from experiments at 80 °C and pCO_2 0.05 MPa with (a) 1,000 ppm Ca^{2+} and (b) 10,000 ppm Ca^{2+}.

it impossible for a protective $FeCO_3$ layer to form.

Focusing on the experiment with initial Ca^{2+} concentration of 1,000 ppm will explain this behavior in more detail. The measured variations of Fe^{2+} concentration and Ca^{2+} concentration with time are plotted in Figure 2(a). The concentration of Ca^{2+} decreased steadily due to precipitation of $CaCO_3$. The Fe^{2+} concentration initially decreased due to precipitation of $FeCO_3$ from a supersaturated solution. Then, as the saturation level was approached, the Fe^{2+} concentration increased due to the high general corrosion rate (Figure 1[a]).

The corresponding saturation degrees with respect to $CaCO_3$ and $FeCO_3$ vs. time are given in Figure 2(b). There, based on the measured pH and Ca^{2+}, the saturation degree with respect to $CaCO_3$ was calculated.

As is shown in Figure 2, because of a very high initial concentration of Ca^{2+}, the aqueous solution was initially highly supersaturated with respect to $CaCO_3$. This led to precipitation of $CaCO_3$ reducing the level of saturation. As the $CaCO_3$ supersaturation level approached 10, the driving force for $CaCO_3$ precipitation decreased and the concentration of calcium changed very slowly. At the same time, the Fe^{2+} concentration initially decreased much more rapidly than the Ca^{2+} concentration even if the initial level of supersaturation with respect to $FeCO_3$ was much lower than that of $CaCO_3$, which points to much faster kinetics. As the level of $FeCO_3$ supersaturation fell below 10, the kinetics of $FeCO_3$ precipitation decreased. At the same time, the corrosion rate remained unchanged (Figure 1[a]), which led to an increase in Fe^{2+} concentration over time.

Figure 3 shows SEM images of specimens from electrolytes with 0 ppm Ca^{2+}, 10 ppm Ca^{2+}, 100 ppm Ca^{2+}, 1,000 ppm Ca^{2+}, and 10,000 ppm Ca^{2+}. The analyses for the

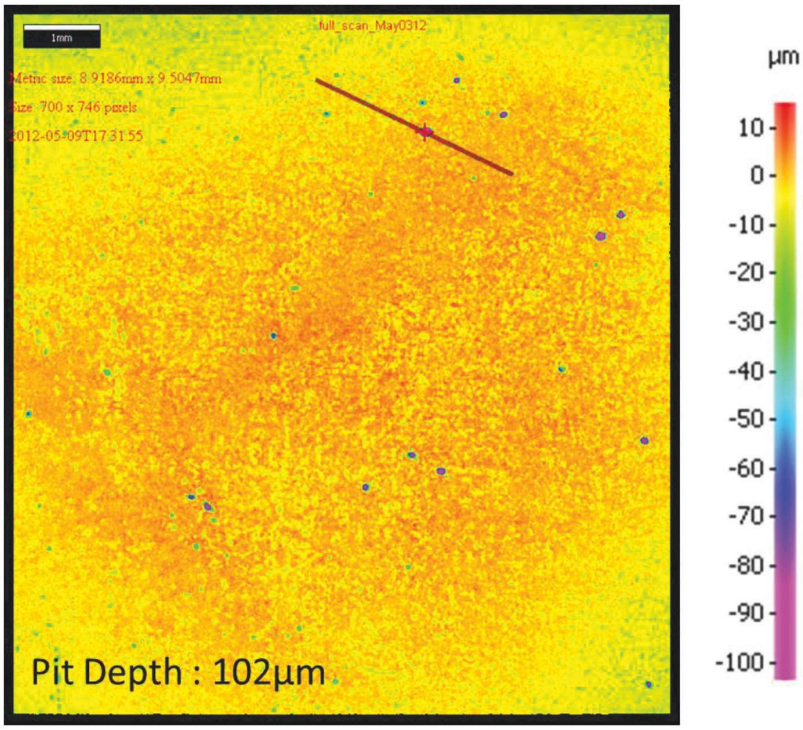

FIGURE 5 IFM of sample (UNS G10180) after removal of corrosion product for the experiment conducted at 80 °C and pCO_2 0.05 MPa with 10 ppm Fe^{2+} + 10,000 ppm Ca^{2+}.

experiments with 0, 10, and 100 ppm Ca^{2+} (Figures 3[a], [b], and [c]) show scattered crystals of $FeCO_3$ on the surface. Corrosion product crystal morphologies did not appreciably change at these relatively low Ca^{2+} concentrations. However, at higher Ca^{2+} concentration, as shown in Figures 3(d) and (e) for 1,000 ppm Ca^{2+} and 10,000 ppm Ca^{2+}, respectively, the crystal morphologies at the surface significantly changed due to the presence of Ca^{2+}. In the experiment with 1,000 ppm Ca^{2+}, the crystals were mostly elongated. For the electrolyte with 10,000 ppm Ca^{2+}, the surface was covered with a dense, intergrown layer of scale rather than being comprised of relatively discrete crystals.

The XRD data of specimens tested with 0 ppm Ca^{2+} and 10 ppm Ca^{2+} confirmed the presence of $FeCO_3$ on the surface. It can be concluded from XRD data on the specimen tested with 10 ppm Ca^{2+} that a thick and protective layer was formed on the surface, as the main peak of α-Fe related to diffraction from the steel substrate cannot be detected. The XRD data show less intense, broadened, and shifted peaks as a result of the substitution of the larger Ca^{2+} for Fe^{2+} in the $FeCO_3$ structure. This causes the formation of a solid solution with the formula $Fe_xCa_yCO_3$, (x + y = 1).

Similar to the experiment condition no. 2 with the addition of 10 ppm Ca^{2+}, the XRD data for the specimen tested with 100 ppm Ca^{2+} again show broadened and shifted peaks relative to $FeCO_3$ with their more profound differences, compared with 10 ppm Ca^{2+} due to the higher concentration of Ca^{2+} in the electrolyte. This is a consequence of greater substitution of Fe^{2+} with Ca^{2+} during formation of the solid solution; compositional complexity and concentration gradients within the $Fe_xCa_yCO_3$ scale are reflected by significant asymmetry in the principle diffraction peaks between 30-32 2θ.

The XRD data for the specimen tested in 1,000 ppm Ca^{2+} are indicative of a transition to a physical mixture of $CaCO_3$ with a solid solution of $Fe_xCa_yCO_3$ on the steel surface. The high corrosion rate in this experiment may be the result of the formation of mostly $CaCO_3$ rather than $FeCO_3$ or $Fe_xCa_yCO_3$ on the surface. This would indicate that $CaCO_3$ is not as protective as $FeCO_3$ or $Fe_xCa_yCO_3$. According to the XRD data for the specimen tested with 10,000 ppm Ca^{2+}, there is a physical mixture of the $CaCO_3$ and a solid solution of $Fe_xCa_yCO_3$ on the surface. The high corrosion rate in this experiment is likely the result of the formation of mostly $Fe_xCa_yCO_3$ with a high concentration of Ca^{2+} on the steel surface.

Figures 4(a) and (b) show the cross section analysis of the tested conditions with 1,000 and 10,000 ppm Ca^{2+}. There is not a significant difference in the layer on the surface between 0 and 10 ppm Ca^{2+}. On the other hand, in the presence of 1,000 ppm Ca^{2+} (Figure 4[a]), two different layers on the steel surface were detected. The concentration of Fe in the layer immediately adjacent to the steel surface is higher than Ca, whereas the layer on the outer surface has the opposite relationship. Taken in conjunction with the cross section analysis, this would imply that a bilayer structure had formed with $CaCO_3$ scale growing from the surface of the $Fe_xCa_yCO_3$ corrosion product. Figure 4(b), the cross section analysis of the experiment with 10,000 ppm Ca^{2+}, does not show an obvious bilayer structure at the steel surface. There is, however, a significant Ca/Fe concentration gradient consistent with the XRD data. There seems to be an increased "roughening" of the steel surface as the Ca^{2+} concentration increases.

SEM images of the surface were obtained after specimens were treated with Clarke solution, which completely removed the surface layer. General roughening of the surface is confirmed as the Ca^{2+} concentration is increased. At the highest Ca^{2+} concentration of 10,000 ppm, there appears to be some initiation of pitting, but this is difficult to judge because of the relatively short duration of the experiments. The calculated maximum penetration rate, according to the deepest pit found by IFM analysis, is 6.0 mm/y, as shown in Figure 5. This is significantly higher than the average uniform corrosion rate detected by LPR (Figure 1[a]).

Conclusions

- The presence of Ca^{2+} affected the corrosion behavior by changing the water chemistry, particularly as the formation of nonprotective $CaCO_3$ interfered with the formation of protective $FeCO_3$.
- The low Ca^{2+} concentration (<100 ppm) did not significantly affect the corrosion rate.

- At a high concentration of Ca^{2+} (≥1,000 ppm), the corrosion behavior was different and high corrosion rates were observed.

Acknowledgments

The authors would like to thank Bruce Brown for his support in this study. The financial support of Ohio University's Department of Chemical and Biomolecular Engineering is appreciated.

References

1 A. Pfennig, A. Kranzmann, "Reliability of Pipe Steels with Different Amounts of C and Cr during Onshore Carbon Dioxide Injection," *Green Gas Control* 5 (2011): pp. 757-769.

2 J. Gale, J. Davison, "Transmission of CO_2—Safety and Economic Considerations," *Energy* 29 (2004): pp. 1,319-1,328.

3 Z. Xian, X. Ming, L. Hong, H. Yong, "Formation Characteristic of CO_2 Corrosion Product Layer of P110 Steel Investigated by SEM and Electrochemical Techniques," *J. Iron Steel Rese. Int.* 16 (2009): pp. 89-94.

4 Z. Xian, L. Ping, H. Ming, L. Hong, L. Lin, "Effect of Ca^{2+} and Mg^{2+} on CO_2 Corrosion Behavior of Tube Steel," *J. Iron. Steel Res. Int.* 12 (2005): pp. 38-42 .

5 C. Ding, K. Gao, C. Chen, "Effect of Ca^{2+} on CO_2 Corrosion Properties of X65 Pipeline Steel," *Int. J. Miner. Metall. Mater.* 16 (2009): pp. 661-666.

6 X. Jiang, Y.G. Zheng, D.R. Qu, W. Ke, "Effect of Calcium Ions on Pitting Corrosion and Inhibition Performance in CO_2 Corrosion of N80 Steel," *Corros. Sci.* 48 (2006): pp. 3,091-3,108.

7 C. Ren, X. Wang, L. Liu, H. Yang, N. Xian, "Lab and Field Investigations on Localized Corrosion of Casing," *Materials and Corrosion* 63 (2012): pp. 168-172.

8 S. Zhu, J. Wei, Z. Bai, G. Zhou, J. Miao, R. Cai, "Failure Analysis of P110 Tubing String in the Ultra-Deep Oil Well," *Engineering Failure Analysis* 18 (2011): pp. 950-962.

9 K. Gao, F. Yu, X. Pang, G. Zhang, L. Qiao, W. Chu, M. Lu, "Mechanical Properties of CO_2 Corrosion Product Scales and Their Relationship to Corrosion Rates," *Corros. Sci.* 50 (2008): pp. 2,796-2,803.

10 ASTM G1-03 (2011), "Standard Practice for Preparing, Cleaning, and Evaluating Corrosion Test Specimens" (West Conshohocken, PA: ASTM International, 2011).

11 S. Nešić, "Key Issues Related to Modeling of Internal Corrosion of Oil and Gas Pipelines—A Review," *Corros. Sci.* 49 (2007): pp. 4,308-4,338.

12 S. Nešić, M. Nordsveen, R. Nyborg, A. Stangeland, "A Mechanistic Model for Carbon Dioxide Corrosion of Mild Steel in the Presence of Protective Iron Carbonate Films—Part 2: A Numerical Experiment," *Corrosion* 59, 6 (2003): pp. 489-497.

This article is based on CORROSION 2013 paper no. 2358, presented in Orlando, Florida.

SABA NAVABZADEH ESMAEELY is a Ph.D. student at the Institute for Corrosion and Multiphase Technology at Ohio University. She has an M.S. degree in chemical engineering from Ohio University. The topic of her thesis is "The Effect of Calcium on the Formation and Protectiveness of Iron Carbonate." She has a B.Sc. degree in mechanical engineering from Bahonar University in Iran. She has been working on corrosion research related to the oil and gas industry for four years and currently works in the area of H_2S/CO_2 corrosion. She is a member of NACE International and the Electrochemical Society.

YOON-SEOK CHOI is a research assistant professor and associate director for research in the Institute for Corrosion and Multiphase Technology at Ohio University. His current research topics are the evaluation of corrosion properties of materials and the development of a corrosion prediction model under high CO_2 pressure environments including oil and gas production/transportation, and CCS processes. He has been a member of NACE International since 2000 and has published 42 reviewed papers in reputable international journals related to corrosion and electrochemistry.

DAVID YOUNG is a research associate professor and assistant director for academic affairs at the Institute for Corrosion and Multiphase Technology at Ohio University. His current research interests include corrosion in CO_2/H_2S environments, CCS, scale deposition, characterization of corrosion products, and zeolite science. He has a Ph.D. from the University of Edinburgh and a B.Sc. degree in chemistry from the University of Dundee. He is a member of the Royal Society of Chemistry and is a Chatered Chemist.

SRDJAN NEŠIĆ, FNACE, is a professor in the Department of Chemical Engineering at Ohio University's Russ College of Engineering and Technology and the director of the university's Institute for Corrosion and Multiphase Flow Technology. He has been involved in corrosion control for more than a decade and has worked as consultant/advisor on corrosion-related projects for the oil and gas industry. Since 2004, Nešić has served on the *Corrosion* editorial board. He received the NACE International H.H. Uhlig Award in 2007 for outstanding effectiveness in post-secondary corrosion education, was named a NACE Fellow in 2008, and received the NACE *Corrosion* Best Paper Award in 2010. He was named the Russ Professor of Engineering at Ohio University in 2010. Nešić holds a Ph.D. from the University of Saskatchewan in Canada, and M.Sc. and B.Sc. degrees in mechanical engineering from the University of Belgrade in Yugoslavia. MP